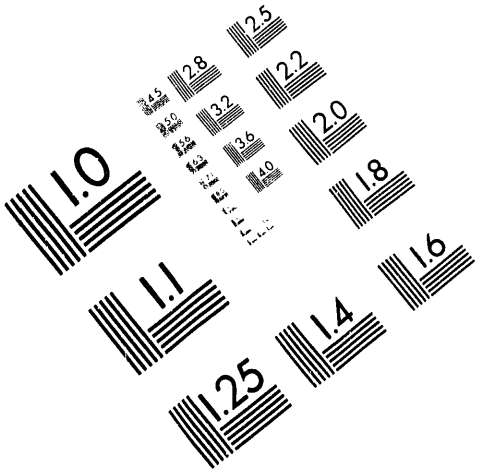

Association for Information and Image Management

1100 Wayne Avenue, Suite 1100
Silver Spring, Maryland 20910

301/587-8202

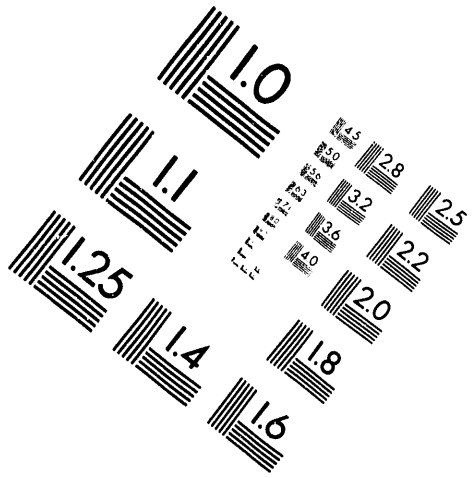

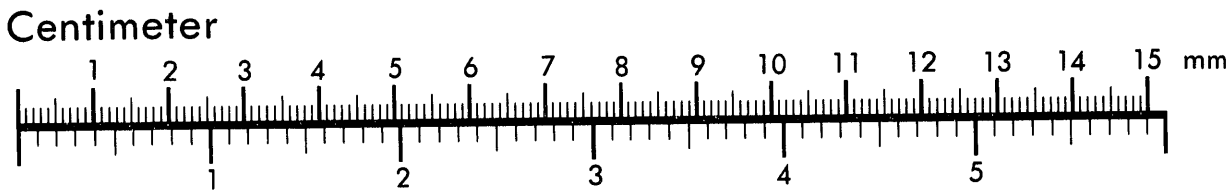

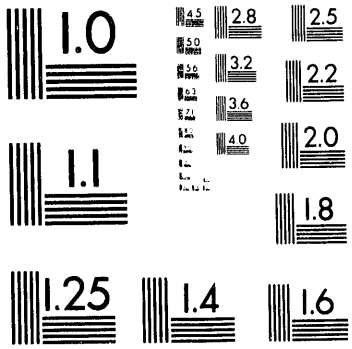

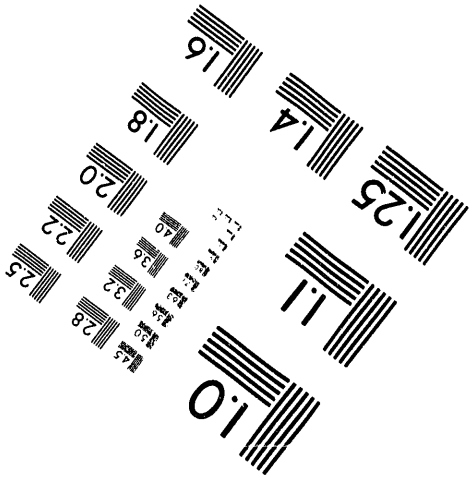

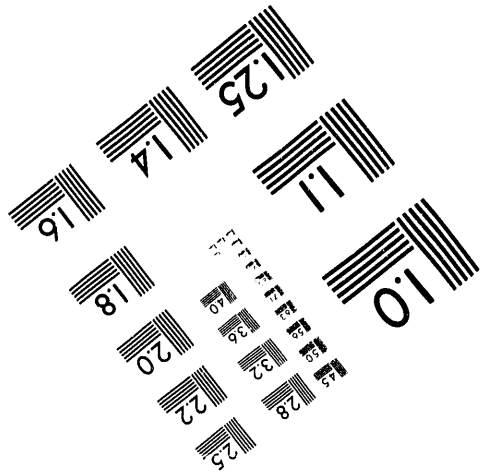

1 of 1

To be presented at the 12th International Corrosion Congress, September 19-24, 1993 in Houston, TX.

Vacancy Condensation as the Precursor to Passivity Breakdown

Digby D. Macdonald
Center for Advanced Materials
The Pennsylvania State University
517 Deike Building
University Park, PA 16802

Abstract

This paper outlines the events that are envisaged to occur, according to the Point Defect Model (PDM), during "chemically-induced" breakdown of the barrier layer on passivated metals and alloys in aqueous environments. The essential hypothesis of the model is that the local generation of cation vacancies at the barrier layer/environment interface, due to the autocatalytic adsorption of a damaging species such as chloride ion into the oxygen vacancy structure, leads to an enhanced flux of cation vacancies across the film. If the vacancies that arrive at the metal/film interface cannot be annihilated by cation ejection from the metal, the vacancies will condense leading to the local decohesion of the barrier layer from the metal. A combination of film dissolution at the barrier layer/environment interface and residual stresses in the oxide film leads to the physical rupture of the film, marking a passivity breakdown event. The PDM accounts for a variety of empircally-established relationships for the nucleation of pits, including the fact that the breakdown voltage (V_c) and induction time (t_{ind}) are distributed quantities; that $V_c = V_c^o$ - blog (a_{Cl^-}), where $b > 2.303RT/F$; and that log (t_{ind}) α $1/\Delta V$, where ΔV = V (applied voltage) - V_c. Also, the model has been extended to account for alloying effects and, indeed, new alloys are now being designed on the basis of rules that have been derived from the PDM.

Introduction

Passivity breakdown is the necessary precursor to localized corrosion of industrially-important metals and alloys. While extensive research has been carried out to ascertain the fundamental aspects of the breakdown phenomenon[1-5], no universally accepted mechanism has been devised. In this paper, the events that occur within the barrier layer leading to "chemically-induced" breakdown, as envisaged in the Point Defect Model (PDM) and the Solute-Vacancy Interaction Model (SVIM)[6-14], are reviewed. We show that the PDM and SVIM are able to account for many of the phenomenological aspects of passivity breakdown and that they lead to a set of rules for designing alloys of enhanced passivity. To our knowledge, these rules represent the first theoretically-inspired procedure for designing new, pitting-resistant alloy systems.

Passivity Breakdown and Pit Nucleation

Structure of Passive Films

The bulk of the experimental evidence indicates that passive films, which form on metals and alloys in contact with aqueous environments, consist of at least two layers, as depicted in Figure 1. The inner or "barrier" layer forms by movement of the metal/film interface into the metal phase, due to the inward movement of oxygen via the outward movement of oxygen vacancies[1]. On the other hand, the outer layer forms by the hydrolysis of cations ejected from the barrier layer at the film/solution interface. Because the barrier layer forms by a solid-state reaction, it is expected to consist of a disordered oxide containing both anion (oxygen) and cation (metal) vacancies, the relative concentrations of which depend on the thermodynamics of vacancy formation and on the kinetics of the vacancy generation and the annihilation reactions (Figure 2).

Key terms: vacancy condensation, passivity breakdown, pitting corrosion, alloy design

Assuming that ions from the environment cannot readily enter the barrier layer via the oxygen vacancy structure, one would not expect the barrier layer to incorporate species from the solution. On the other hand, the outer layer can readily incorporate ions from the environment via coprecipitation, so that the oxide, oxyhydroxide, or hydroxide that comprises the outer layer is expected to contain extraneous species from the environment. This is perhaps best seen in the case of aluminum when anodized in borate buffer solutions, where borate ions are found to be incorporated into the outer layer but are absent from the inner layer[15].

Pitting Corrosion. The best known causative agent of "chemically-induced breakdown" is chloride ion, which shows a remarkable ability to cause pitting on many metals and alloys of industrial interest[16-18]. Assuming that an ion, like chloride, must interact physically with the barrier layer to cause passivity breakdown, and hence to nucleate pits, it is of interest to explore, for the moment, how this might happen on an atomistic scale. Accordingly, it is necessary to envisage oneself as a hydrated chloride ion ($Cl^- \cdot nH_2O$, $n \approx 6$) approaching the film/solution interface of the barrier layer (after moving through the precipitated, outer layer). From this vantage point, the barrier layer appears as an undulating surface of charge with positive potentials occurring over cations and negative potentials over anions, with the difference between the peaks depending on the degree of covalent (vs. ionic) bonding in the lattice (the greater the extent of covalent bonding the lower the difference between peaks). Occasionally, however, the chloride ion will experience vacancies, with cation vacancies appearing as sites of high negative charge (corresponding to a formal charge of $-\chi e$) and oxygen vacancies appearing as sites of high positive charge (formally +2e). Thus, the chloride ion is presented with a number of attractive sites to attack, but which will be favored? This is a very difficult question to answer unequivocally, because other processes must be considered. For example, a chloride ion could absorb into a surface oxygen vacancy, but this must be done at the expense of considerable dehydration. However, the high coordination afforded by neighboring ions is a positive factor (favoring absorption), although any expansion of the vacancy to accommodate the ion would be energetically costly. On the other hand, the anion could interact electrostatically with a positive center in the film surface represented by a surface cation; in this case, the interaction might be weaker (because of significant covalent bonding) but, because less dehydration is required in that the ion would not penetrate into the surface, the overall effect might favor absorption at a cation site. These two scenarios could lead to quite different mechanisms for localized attack.

In the first case (anion absorption into a surface oxygen vacancy), the film may respond in a number of different ways, as depicted in Figure 3. In one way (Case I), the system responds to the loss of oxygen vacancies by generating cation vacancy/oxygen vacancy pairs via a Schottky-pair type of reaction. The oxygen vacancies in turn react with additional anions (e.g. chloride) at the film/solution interface to generate yet more cation vacancies. Importantly, the generation of cation vacancies is autocatalytic, but whether or not the film breaks down depends on the relative rates with which the cation vacancies are transported across the barrier layer and are annihilated by emission of cations from the metal into the film. If this annihilation reaction is incapable of consuming the cation vacancies arriving at the metal/film interface, the excess vacancies will condense and lead to the local detachment of the film from the underlying metal, as depicted in Figure 4. Consequently, provided the local tensile stresses are sufficiently high and/or the film dissolves locally, the barrier layer will rupture, marking the initiation of a pit. The evidence for this mechanism is discussed elsewhere[1].

This particular case was considered in detail by Lin et al[6], who assumed that the enhanced flux of cation vacancies across the barrier layer could not be accommodated by Reaction (1) in Figure 2, thereby leading to the formation of a cation vacancy condensate. Once the condensate (Figure 4) has grown to a critical size, dissolution of the film at the film/solution interface and the tensile stresses in the barrier layer induce a mechanical or structural instability, resulting in rupture of

the film and hence in rapid localized attack. These ideas were assembled by Lin et al[6] to derive expressions for the critical breakdown voltage and induction time for a single breakdown site as

$$V_c = \frac{4.606RT}{\chi F\alpha}\log\left[\frac{J_m}{J^o\, u^{-\chi/2}}\right] - \frac{2.303RT}{\alpha F}\log\left(a_{X^-}\right) \tag{1}$$

and

$$t_{ind} = \xi'\left[\exp\left(\frac{\chi F\alpha\Delta V}{2RT}\right) - 1\right]^{-1} + \tau \tag{2}$$

where ΔV is the breakdown overvoltage ($\Delta V = V - V_c$), a_{X^-} is the activity of X^- in the solution,

$$\xi' = \xi / J^o\, u^{-\chi/2}\left(a_{X^-}\right)^{\chi/2}\exp\left(\frac{\chi\alpha FV_c}{2RT}\right) \tag{3}$$

and ξ is the critical areal concentration of cation vacancies at the metal/film interface. Other parameters are as defined in the original publication[6]. Equations (1) and (2) account for many of the phenomenological characteristics of pitting attack; (i) that the "pitting potential" (V_c) varies linearly with $\log(a_{X^-})$ with a slope greater than 2.303RT/F (i.e. > 0.05916V/decade at 25°C) because $\alpha < 1$, (ii) that $\log(t_{ind}) \propto 1/\Delta V$ for sufficiently large overvoltages, and (iii) that t_{ind} is an inverse function of the activity of the aggressive anion.

In deriving Equations (1) and (2), we have assumed that the critical concentration of cation vacancies at breakdown (ξ mol. vacancies/cm^2) is independent of the applied voltage and hence thickness of the barrier layer. This assumption was made because transmission of cation vacancies through the film can occur only as long as the film is attached to the base metal in order that the vacancies can be annihilated by Reaction (1), Figure 2 (see also Figure 4). Thus, growth of the condensate normal to the interface cannot occur once the film has separated from the substrate and, since separation occurs by condensation of a single layer of vacancies, our assumption of $\xi \neq f(V,L)$ is justified.

Distribution Functions. On any real surface, a large number of potential breakdown sites exist corresponding to a distribution in the properties of the "weak spots". Perhaps the most graphic illustration of this property is the data of Shibata and co-workers[19,20], who showed that the "pitting potential" is near normally distributed and that the induction time follows a distribution that is skewed towards short times. Assuming that the breakdown sites on a surface are normally distributed with respect to the cation vacancy diffusivity, we derived distribution functions for the breakdown voltage and induction time of the form[10,11†]

$$\frac{dN}{dV_c} = -\frac{\gamma D}{\sqrt{2\pi}\,\sigma_D}\, e^{-(D-\bar{D})^2/2\sigma_D^2} \tag{4}$$

and

$$\frac{dN}{dt_{ind}} = \left[\frac{\xi u^{\chi/2}}{\sqrt{2\pi}\,\sigma_D\,\hat{a}}\right] e^{-(D-\bar{D})^2/2\sigma_D^2} \cdot \frac{e^{-\gamma V}}{a_x^{\chi/2}\left(t_{ind}-\tau\right)^2} \tag{5}$$

† Equations [6] and [7] are given in slightly different form in Refs. 10 and 11.

where $\gamma = \alpha\chi F/2RT$, σ_D is the standard deviation for the diffusivity for the population of breakdown sites, and the other quantities are as previously defined[10,11].

For comparison with experiment, we define the cumulative probability in the breakdown voltage and the differential cumulative probability in the induction time as

$$P(V_c) = 100 \int_{-\infty}^{V_c} \left(\frac{dN}{dV_c}\right) dV_c \tag{6}$$

and

$$\Delta N \Big]_{t_j}^{t_{j+1}} = \int_{t_j}^{t_{j+1}} \left(\frac{dN}{dt_{ind}}\right) dt_{ind} \tag{7}$$

The latter quantity is defined in this manner so that direct comparison can be made with experimental pitting induction time data, which are commonly presented as histograms of the number of pits nucleating in successive increments of time.

A fit of $P(V_c)$ to the experimental data of Shibata et al[19,20] for pitting of Fe-17Cr in 3.5% NaCl solution at 30°C is shown in Figure 5. This fit was accomplished by adjusting groups of unknown or poorly-known parameters, which affect the location of $P(V_c)$ on the potential axis but not the shape, such that the experimental and calculated distribution functions coincide for a mean diffusivity for cation vacancies of 5×10^{-20} cm^2/s (this is approximately the value indicated by electrochemical impedance spectroscopy). Without adjusting any additional parameters, the distribution (histogram) in induction time is found to agree very well with the experimental data for the same system, as shown in Figure 6. It should be noted that the model described thus far does not consider the "death" or repassivation of pits; however, its omission is appropriate because, in Shibata's analyses, each specimen was taken out of the population once breakdown had occurred. We should also note that similar distributions in V_c and t_{ind} are obtained if we assume other distribution functions (e.g. the student-t and χ^2 distributions) for the breakdown sites with respect to cation vacancy diffusivity.

The analysis outlined above has permitted us to identify factors that make for "good passivity." Besides lowering the total number of potential breakdown sites per unit area of the surface, the parameter that may be manipulated to impact the susceptibility of a passive film to chemically-induced breakdown is the cation vacancy diffusivity. Thus, a decrease in the cation vacancy diffusivity results in an increase in the "pitting potential" (i.e. $\overline{V}_c$), because a higher voltage is required to produce the same flux of cation vacancies across the barrier layer. Note that metals that have inherently low cation vacancy diffusivities (e.g. Ti, Zr, Ta) are quite resistant to pitting.

The Theory of Alloys

The development of a successful theory for the effects of alloying on corrosion resistance would have an enormous impact on how alloys are designed, particularly if the theory is quantitative and, hence, deterministic. Significant progress has been made towards that goal with the development of the Solute-Vacancy Interaction Model (SVIM) by Urquidi-Macdonald and Macdonald[1,13] some years ago. Although this model has now been extended to account for the effects of alloying elements on the distributions in V_c and t_{ind}, it is currently limited to dilute binary alloys. Nevertheless, the SVIM has led to the derivation (to our knowledge) of the first theoretically-inspired set of rules for choosing an alloying element, as discussed later in this paper.

Segregation of Alloying Elements. In the analysis that follows, we assume that the alloying element is uniformly distributed throughout the metal phase. Accordingly, the reactions that occur within the metal/solution interphase (as depicted in Figures 1–3) lead to non-uniform distributions of the elements within the metal (but close to the interface), the barrier layer, and perhaps even in the precipitated outer layer normal to (but not latterally across) the surface. That alloying elements are segregated into the barrier layer (but not necessarily into the upper, precipitated layer) is shown unequivocally by the SALI (Surface Analysis by Laser Ionization) data presented in Figure 7[21]. These data show that, for a series of Ni-A alloys, with A = Al, Ti, and Mo, the extent of segregation of the alloying element into the barrier layer increases with increasing charge on the solute (i.e. Ni-Al < Ni-Ti < Ni-Mo, for which the solutes may be represented as $Al_{Ni}^{\bullet}$, $Ti_{Ni}^{2\bullet}$, and $Mo_{Ni}^{4\bullet}$). Furthermore, it is evident from the existence of the diffusion gradient of the alloying element in the alloy phase that segregation occurs via a solid state reaction at the metal/film interface, as discussed below. The greater segregation of more highly charged solutes into the barrier layer can be explained in terms of the more favorable free energy of these species in the high dielectric film (for example, experimental measurements indicate that the dielectric constant for the passive film on Cr is ≈ 56 whereas that on Type 304SS is 68-107, see citations in Ref. 11), compared with that for a less highly charged species.

Extensive work on the segregation of chromium into the passive films that form on Fe/Cr alloys in acidic and alkaline solutions has been reported by Strehblow and coworkers[22-24] and by others[25-27]. Using a combination of XPS (X-ray Photoelectron Spectroscopy) and ISS (Ion Scattering Spectroscopy), Strehblow et. al[22-24] found that the inner ("barrier") layers of the passive films formed on Fe-XCr (X = 5–20%) were substantially enriched in chromium, whereas the outer layers were enriched in Fe(III). For passive films formed under identical conditions (mechanical polishing followed by passivation in 0.5M H_2SO_4 for 3 hours at 0.9 V vs. SHE) the segregation factor [$S = (X_{Cr}^{film}/X_{Fe}^{film}) / (X_{Cr}^{alloy}/X_{Fe}^{alloy})$] decreases from ~ 14 for the Fe-5Cr alloy to ~8 for Fe-20Cr, as calculated from the data given in Figure 3 of Ref. 22. Furthermore, for passive films formed for 5 minutes on Fe-15Cr in 1M NaOH, the segregation factor was found to decrease slightly with increasing formation voltage, from ~3 at –0.86V (SHE) to ~2.2 at 0.34V (SHE). A similar trend with formation voltage was found in our work[21] for the Ni-A (A=Al, Ti, Mo) alloys referred to above, although no clear trend in the segregation factor with concentration of A in the alloy could be discerned. A comprehensive theory for the segregation of alloying elements into the barrier layers formed on alloys, on polarization in aqueous systems, has yet to be developed, so that a quantitative interpretation of the findings discussed above is not possible. In the analysis that follows, we will accept segregation as an experimentally demonstrated phenomenon, with the caveat that it is not yet possible to calculate, on an *a priori* basis, the concentration of alloying element in the barrier layer from the composition of the alloy. Accordingly, all "compositions" referred to in the remainder of this paper will be those for the barrier layer.

Solute-Vacancy Interaction Model. Returning now to the role of alloying elements in passivity breakdown, we proposed[12] that the interaction between the substitutionally present (immobile) solute and mobile cation vacancies can be represented as a chemical equilibrium,

$$A_M^{(n-\chi)\bullet} + qV_M^{\chi'} \xleftrightarrow{K_q} \left[A_M \left(V_M^{\chi'}\right)_q\right]^{[n-\chi(1+q)]\bullet} \tag{8}$$

where n is the oxidation charge of the solute (e.g. +6 for Mo^{6+}), and K_q is the equilibrium constant. For 1:1 complexes, Urquidi-Macdonald and Macdonald[11] derived the modified vacancy diffusivity as

$$D^* = \frac{D}{2}\left[1 \mp \frac{(\hat{\alpha} - n_A)}{\left(\hat{\alpha}^2 - n_A n_V\right)^{1/2}}\right] \tag{9}$$

and a modified K* (= εF/RT) as

$$K^* = 2K\frac{\left[1 - \hat{\alpha}/n_V \mp \left(\hat{\alpha}^2 - n_A n_V\right)^{1/2}/n_V\right]}{\left[1 \mp (\hat{\alpha} - n_A)/\left(\hat{\alpha}^2 - n_A n_V\right)^{1/2}\right]} \tag{10}$$

where $\hat{\alpha} = (n_A + n_V + K_1^{-1})/2$, and n_A and n_V are the stoichiometric concentrations of the solute and cation vacancies in the film. By applying ion-pairing theory, as used in solution theory and in solid state physics, we can express the equilibrium constant, K_1, as

$$K_1 = \left[4\pi(t/kT)^3 \int_a^{-t/2kT} e^{\gamma}\,\gamma^2\,d\gamma\right] \tag{11}$$

where a is the distance of closest approach, $t = z_1 z_2\, e^2/\hat{\varepsilon}\hat{\varepsilon}_o$, z_1 and z_2 are the charges (including signs) on the interacting species, e is the electron charge, $\hat{\varepsilon}$ is the dielectric constant, $\hat{\varepsilon}_o$ is the permitivity of free space, and γ is the variable of integration. The equilibrium constant, K_1, needs to be corrected for screening by the mobile vacancies. This correction is expressed through Debye-Huckel theory as[12]

$$K_1^{corr} = K_1\, f_A\, f_M \tag{12}$$

where f_A and f_M are activity coefficients given by

$$f_A = \exp\left\{-\frac{e^2 z_2^2}{2\hat{\varepsilon}\hat{\varepsilon}_o T \ell_D (1 + b'/\ell_D)}\right\} \tag{13}$$

and

$$f_M = \exp\left\{-\frac{e^2 z_1^2}{2\hat{\varepsilon}\hat{\varepsilon}_o kT \ell_D (1 + b'/\ell_D)}\right\} \tag{14}$$

The parameter ℓ_D is the Debye length

$$\ell_D = \left\{\frac{\hat{\varepsilon}\hat{\varepsilon}_o\, kT}{e^2 4\pi\left[n_V z_1^2 + n_A z_2^2\right]}\right\}^{1/2} \tag{15}$$

and b′ is the distance at which the coulombic interaction energy is equal to kT (the thermal energy)

$$b' = -\frac{z_1 z_2 e^2}{2\hat{\varepsilon}\hat{\varepsilon}_o\, kT} \tag{16}$$

Although the SVIM is currently quite crude, in that it does not consider the complexing of more than one cation vacancy per solute and does not employ exponential distributions of vacancies across the film, the model is surprisingly successful in accounting for the effect of molybdenum, for example, on the pitting characteristics of stainless steel. Thus, by combining the SVIM with the distribution functions for passivity breakdown, we calculated $P(V_c)$ as a function of molybdenum concentration in the alloy, assuming that the solute is in the +6 oxidation state (we have also considered the +4 state but it will not be discussed extensively here), and that preferential segregation of Mo into the barrier layer did not occur (i.e. the concentration of Mo in the barrier layer was assumed to be the same as that in the base alloy). The distribution functions are shown in Figure 8. In deriving these data, we selected model parameters so that the molybdenum-free case coincided with the experimental data of Shibata[19,20] for Fe-17Cr in 3.5% NaCl at 30°C; these parameters were then maintained constant for all molybdenum-containing alloys. Accordingly, as far as the latter are concerned, there are no arbitrarily adjustable parameters in the model.

The $P(V_c)$ data plotted in Figure 8 predict that small additions of molybdenum (e.g. 1%) have only a modest impact on the pitting characteristics of stainless steel, but that additions of greater than 2% have a large impact. However, additions of more than 3% have incrementally smaller effects, at least for the parameter values chosen for these calculations. In this regard, it is interesting to note that experience has shown that 2 - 2 1/2% Mo is optimal for protecting Type 304SS against pitting in seawater systems with the modified alloy being the well-known Type 316SS. Perhaps a better test of the SVIM is afforded by the data plotted in Figure 9, where a comparison of $\overline{V}_c$ (breakdown voltage at the 50th percentile) is made with experimental data from the literature. Although the experimental data do not display the sigmoid shape predicted by theory (and probably could not because of their limited precision), the agreement between experiment and theory is surprisingly good. Also shown is the prediction of the SVIM assuming that molybdenum is in the +4 state; clearly, the former (Mo^{6+}) provides a better description of the experimental data than does the latter (Mo^{4+}), although the actual oxidation state of molybdenum in the barrier layer on stainless steel has not been established unequivocally. The major impact of shifting $P(V_c)$ in the positive direction is to greatly increase the induction time for passivity breakdown (i.e. the time required to accumulate a critical concentration of cation vacancies at the metal/film interface). Although we do not show the calculations here, this is precisely what is predicted by the model.

Other data also support the predictions of the model. For example, various studies[3-5] on supersaturated aluminum alloys of the type Al-A (A = 0-8 a/o Mo, Cr, Ta, W) have shown that elements such as molybdenum and, in particular, tungsten, can displace the critical potential for pitting in chloride solution in the positive direction by as much as 2500mV(4). Both elements form species in the +6 oxidation state, which should complex mobile $V_{Al}^{3'}$ vacancies, although the extensive segregation of the alloying element into the barrier layer has not been demonstrated. However, in the presence of a thick outer layer (relative to the barrier layer), even when using a glancing radiation technique (e.g. EXAFS), as employed in those studies[3-5], it is difficult to establish the extent of segregation into the barrier layer alone, and it is likely that techniques with much higher depth resolution, such as SALI, will be required to fully characterize the composition of the interfacial region.

Alloy Design

What makes a good alloy? An answer to this question is of enormous scientific, technological, and economic importance, given that the annual cost of corrosion in any industrial society is about 4.5% of the GNP (about $230 billion for the US in 1990). The work outlined above

provides clear guidance on this question and, recognizing that the models are still quite crude, we have formulated a set of principles to aid the alloy designer in devising new systems of superior resistance to passivity breakdown. The rules are as follows:

(i) The alloying element must segregate into the barrier layer, preferably preferentially with respect to the host cation.

(ii) The alloying element must exist in a "dissolved" (substitutional) state in the barrier layer in as high an oxidation state as possible, and certainly in an oxidation state that is higher than that of the host cation.

(iii) The alloying element should be uniformly distributed throughout the layer or at least should not form a second phase that might introduce heterogeneities into the barrier layer that could act as sites for the nucleation of localized attack.

Other factors also affect the theoretical effectiveness of an active alloying element, according to the SVIM. For example, a decrease in the dielectric constant (Figure 10) and a decrease in the distance of the closest approach [Equation (13)] will both shift Reaction (8) to the right, signifying stronger interaction between the ionized alloying element ($A_M^{(n-\chi)\bullet}$) and the mobile cation vacancies. However, neither of these parameters are readily manipulated, so that their optimization is not included in the rules outlined above.

We have tested these principles by measuring distribution functions, $P(t_{ind})$, for a series of Ni-xAl, Ni-xTi, and Ni-xMo alloys (x = 0-8 atomic %) in NaCl/borate buffer solutions at 25°C[29]. In these experiments, the specimens were held at a constant potential above the "pitting potential," and the number of pits nucleated on the surface were counted as a function of time. Although these experiments are complicated by the observation that existing active pits protect the remaining surface at radii that increase with time (and for this reason they have not yet been published), the data are in good qualitative agreement with the predictions of the model, in that the Ni-Mo alloys were the most resistant and the Ni-Al alloys were the least resistant to passivity breakdown, with the effect being roughly as expected from the charge on the solute (i.e. 4: 2: 1 for $Mo_{Ni}^{4\bullet}$: $Ti_{Ni}^{2\bullet}$: $Al_{Ni}^{\bullet}$).

Acknowledgements

The authors gratefully acknowledge the support of this work by the U.S. Department of Energy, Division of Basic Energy Sciences, under Grant No. DE-DG03-84ER45461.

References

1. D.D. Macdonald, J. Electrochem. Soc., 139, 3434 (1992).

2. A.J. Sedriks, Corrosion of Stainless Steels, The Electrochemical Soc., Princeton, NJ (1979).

3. B.A. Shaw, G.D. Davis, T.L. Fritz, B.J. Rees, and W.C. Moshier, J. Electrochem. Soc., 138, 3288 (1991).

4. G.D. Davis, W.C. Moshier, G.G. Long, and D.R. Black, J. Electrochem. Soc., 138, 3194 (1991).

5. P.M. Natishan, E. McCafferty, and G.K. Hubler, J. Electrochem. Soc., 133, 1061 (1986); 135, 321 (1988).

6. C.-Y. Chao, L.-F. Lin, and D. D. Macdonald, J. Electrochem. Soc., 128, 1187 (1981); 128, 11 (1981); 129, 1874 (1982.

7. D. D. Macdonald and M. Urquidi-Macdonald, J. Electrochem. Soc., 137, 2395 (1990).

8. D. D. Macdonald, S. Biaggio, and H. Song, J. Electrochem. Soc., 139, 170 (1991).

9. D. D. Macdonald, S. I. Smedley, Electrochim. Acta., 35, 1949 (1990).

10. D. D. Macdonald and M. Urquidi-Macdonald, Electrochim. Acta., 31, 1070 (1986).

11. M. Urquidi-Macdonald and D. D. Macdonald, J. Electrochem. Soc., 134, 41 (1987).

12. M. Urquidi-Macdonald and D. D. Macdonald, J. Electrochem. Soc., 136, 961 (1989).

13. D. D. Macdonald and M. Urquidi, J. Electrochemical Soc., 132, 555 (1985).

14. S. Lenhart, M. Urquidi-Macdonald, and D. D. Macdonald, Electrochim. Acta, 32, 1739 (1987).

15. G.C. Wood and J.P. O'Sullivan, J. Electrochem. Soc., 116, 1351 (1969).

16. "Passivity and Its Breakdown on Iron and Iron-Based Alloys," R. W. Staehle and H. Okada (Editors), NACE, Houston, TX (1976).

17. "Passivity of Metals and Semiconductors," M. Fromout (Editor), Elsevier, Amsterdam (1983).

18. "Passivity of Metals," R. P. Frankenthal and J. Kruger (Editors), the Electrochemical Society, Princeton, NJ (1978).

19. T. Shibata, Trans. ISIJ, 23, 785 (1983).

20. T. Shibata and T. Takeyama, Corrosion, 33, 243 (1977).

21. D.D. Macdonald, M. Ben-Hain, and J. Pallix, J. Electrochem. Soc., 136, 3269 (1989).

22. C. Calinski and H.-H. Strehblow, J. Electrochem. Soc., 136, 1328 (1989).

23. S. Haupt and H.-H. Strehblow, Corr. Sci., 29, 163 (1989).

24. S. Haupt, C. Calinski, U. Collisi, H.W. Hoppe, H.-D. Speckmann, and H.-H. Strehblow, Surf. Interf. Anal., 9, 357 (1986).

25. R.P. Frankenthal and D.L. Malm, J. Electrochem. Soc., 123, 186 (1976)

26. S. Storp and R. Holm, Surf. Sci., 68, 10 (1977).

27. K. Asami, K. Hashimoto, and S. Shimodaira, Corr. Sci., 16, 387 (1976).

28. E.A. Lizlovs and A.P. Bond, J. Electrochem. Soc., 122, 720 (1975).

29. D.D. Macdonald, C. English, and S.J. Lenhart, unpublished data (1985).

DISCLAIMER

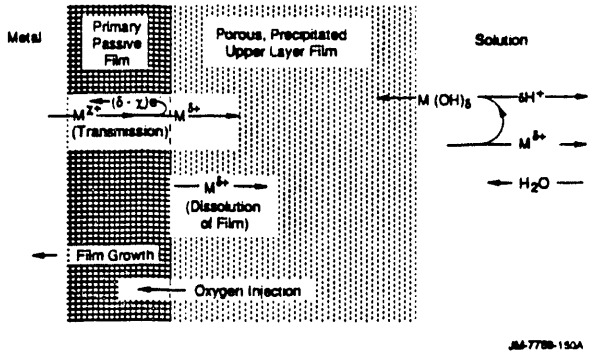

Figure 1. Schematic of processes that lead to the formation of bilayer passive films on metal surfaces.

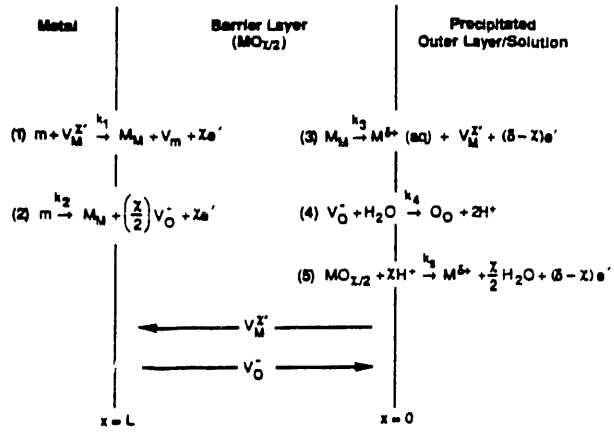

Figure 2. Schematic of physico-chemical processes that occur within the barrier layer according to the point defect model.

m = metal atom, M_M = metal cation in cation site, O_O = oxygen ion in anion site, $V_M^{\chi'}$ = cation vacancy, $V_O^{\cdot\cdot}$ = anion vacancy, V_m= vacancy in metal phase.

During film growth, cation vacancies are produced at the film/solution interface, but are consumed at the metal/film interface. Likewise, anion vacancies are formed at the metal/film interface, but are consumed at the film/solution interface. Consequently, the fluxes of cation vacancies and anion vacancies are in the directions indicated. Note that Reactions [1], [3], and [4] are lattice conservative processes, whereas Reactions [2] and [5] are not.

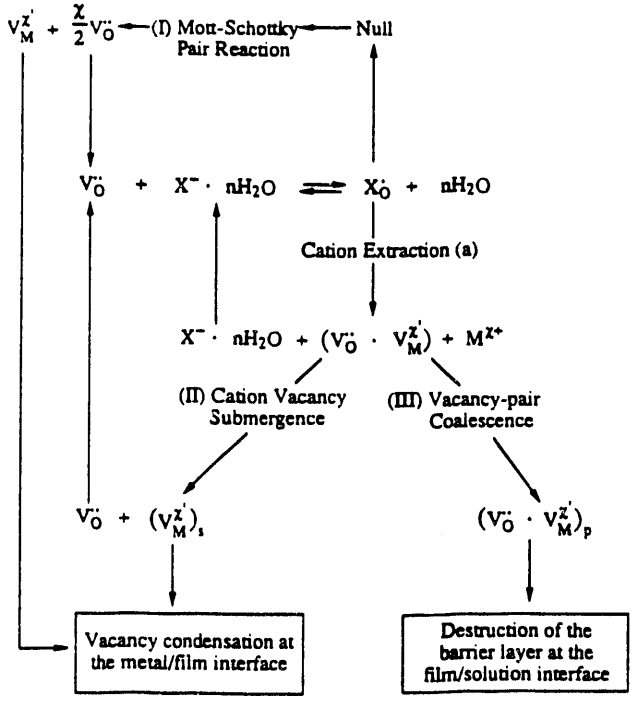

Figure 3. Summary of proposed reactions leading to passivity breakdown.

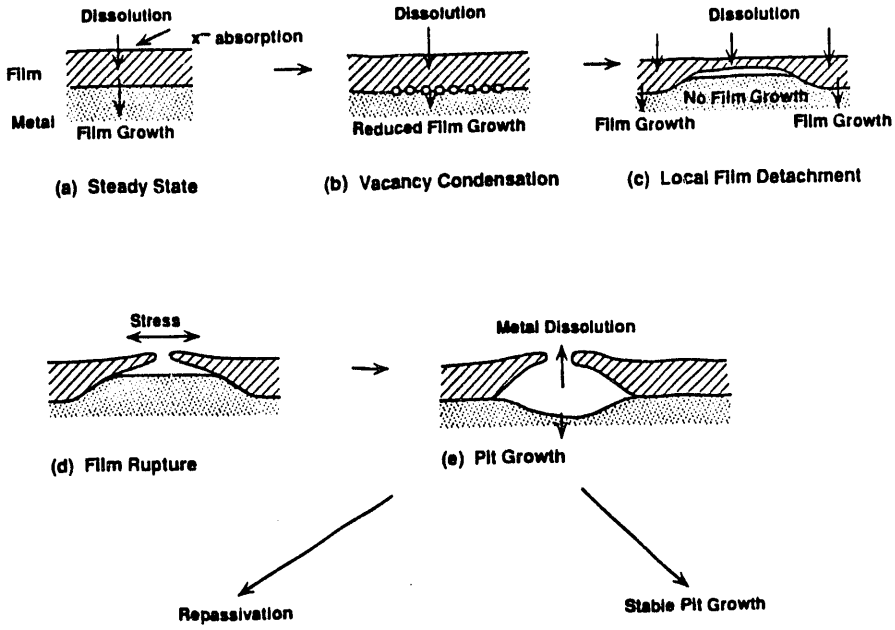

Figure 4. Cartoon outlining various stages of pit nucleation according to the Point Defect Model

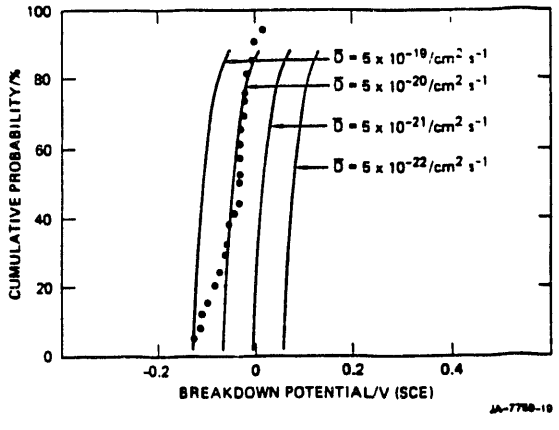

Figure 5. Cumulative probabilities for the breakdown voltage as a function of $\overline{D}$ for normal distributions in the diffusivity D.

σ_D = 0.75. *Data for Fe-17Cr in 3.5% NaCl solution at 30°C from Shibata [19,20]. $\overline{V}_c$ = -0.046 V (SCE).

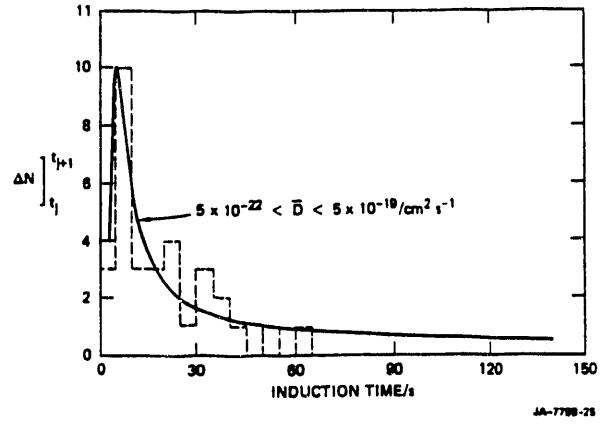

Figure 6. Differential cumulative probabilities for the induction time as a function of $\overline{D}$ for normal distributions in D.

σ_D =0.75 $\overline{D}$. (----) Data for Fe-17Cr in 3.5% NaCl solution at 30°C from Shibata [19,20]. $\overline{V}_c$ = -0.046 V (SCE), V = 0.020 V (SCE), t = 7.5 s, τ = 0.

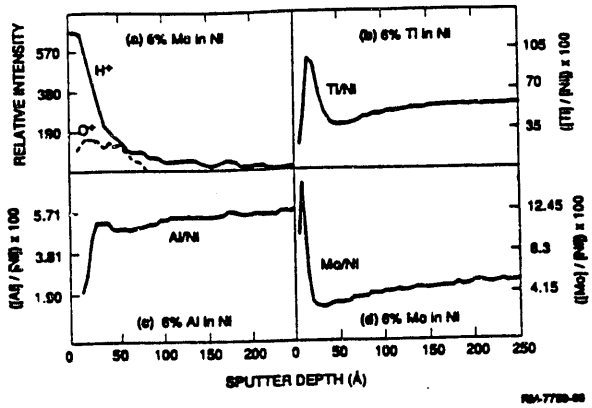

Figure 7. Concentration profiles of H, O, Al, Ti, and Mo in passive films formed on Ni-6% Al, Ni-6% Ti, and Ni-6% Mo in 0.1N H_3PO_4/NaOH, pH = 12, at 25°C as determined by surface analysis by laser ionization. V = 0.30V vs. SCE, growth time = 12 h (21).

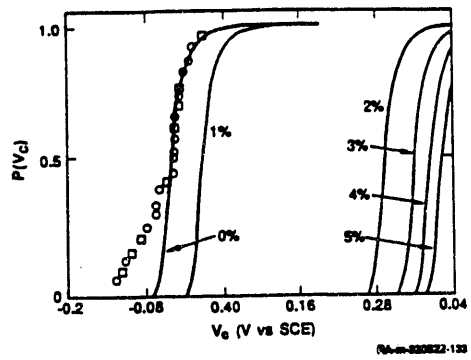

Figure 8. Effect of solute (Mo) concentration (n_{Mo}·wt%) on the cumulative distribution function for V_c for a passive film containing 6^+-3^- complexes.

$n_V = 5 \times 10^{20}$ cm^{-3}, $K_1 = 1.13 \times 10^{-16}$ cm^3. O, ❑ Data of Shibata [19,20] for Fe-17Cr in 3.5% NaCl at 30°C.

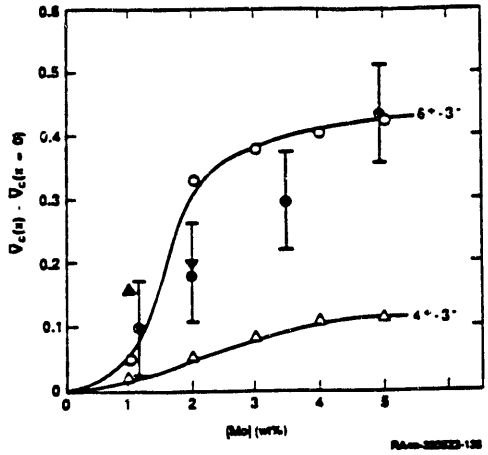

Figure 9. Effect of molybdenum concentration on $V_c(x) - V_c(x=0)$ for 6^+-3^- (O) and 4^+-3^- (Δ) complexes in the film.

$n_V = 5 \times 10^{20}$ cm^{-3}, $K_1 = 1.13 \times 10^{-16}$ cm^3 (O), $K_1 = 9.05 \times 10^{-21}$ cm^3 (Δ).

- ● Lislovs and Bond [28]: Fe-18Cr in 1M NaCl at 25°C
- ▲ Shibata [19]: Fe-17Cr in 3.5% NaCl at 30°C
- ▼ Shibata [20]: Fe-18Cr in 3.5% NaCl at 30°C

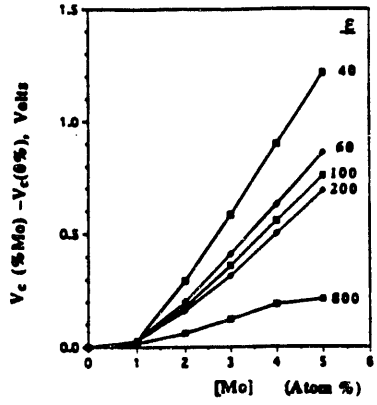

Figure 10. Calculated shift in the mean critical breakdown potential with molybdenum concentration in the barrier layer as a function of the dielectric constant.

[$\Omega = 30$ cm^3/mol, $\Delta G_{A\text{-}1} = -4 \times 10^4$ J/mol, $\phi^o_{f/s} = -0.5$V, $\Delta G^o_s = -4 \times 10^4$ J/mol, $\tau = 0$, $D = 5 \times 10^{-20}$ cm^2/s, $n_v = 5 \times 10^{20}$ cm^{-3}, $\varepsilon = 1.1 \times 10^6$ V/cm, T = 303.15 K, $\alpha = 0.65$, $\beta = -0.01$, pH = 7, $a_{x^-} = 0.402$, $\xi = 1.0 \times 10^{16}$ cm^{-2}, $J_m = 1.587 \times 10^{13}$/cm^2.s, $N_o = 5000$ cm^{-2}]

DATE
FILMED
8/17/93

END